A&A 405, 909–915 (2003)
DOI: 10.1051/0004-6361:20030587

Astronomy & Astrophysics

Spectral activity of the Seyfert galaxy Markarian 6 in 1970–1991

V. T. Doroshenko[1] and S. G. Sergeev[2]

[1] Crimean Laboratory of the Sternberg Astronomical Institute, University of Moscow, Russia; P/O Nauchny, 98409 Crimea, Ukraine
Isaac Newton Institute of Chile, Crimean Branch
[2] Crimean Astrophysical Observatory, P/O Nauchny, 98409 Crimea, Ukraine
Isaac Newton Institute of Chile, Crimean Branch
e-mail: sergeev@crao.crimea.ua

Received 10 December 2002 / Accepted 21 March 2003

Abstract. We present results of the reduction of the archive spectra of the nucleus of Mrk 6 obtained in 1970–1991 using the image tube spectrograph at the 2.6-m Shajn telescope of the Crimean Astrophysical Observatory. We analyze 363 spectra for 181 dates obtained in the Hβ spectral region. The spectra in the Hα region (194 spectra for 179 dates) were used to get light curves. The light curves in the Hβ and Hα lines and also in the adjacent continuum show appreciable variability. Broad-line profile parameters (such as centroid, width, blue-to-red ratio of fluxes) seem to be independent of or dependent very weakly on the continuum flux. However, there is a tendency for the blue-to-red ratio of fluxes to increase with increasing continuum flux, and also a weak tendency for the profile width (profile dispersion) to decrease with increasing continuum flux. An anti-correlation between Hβ shapes at the blue and red wings, positive correlation between blue shape and line/continuum flux, and anti-correlation between red shape and line/continuum flux show that the blue segments respond slightly better to the continuum changes than the red segment and total Hβ line. We assume that the observed broad profile consists of at least two components with fixed profiles. We found that one of the components is nearly symmetric and has a single peak, while the other component has a blue bump and extended red wing. In terms of such a two-broad-components profile model, the evolution of the observed Hβ profiles can be roughly reproduced by changes in the relative strength of the two variable components. However, the evolution of the broad Hβ profile in Mrk 6 is complicated and not clear at all. The evolution is driven, most likely, by a set of various factor, including a multi-component BLR model with redistribution of ionizing radiation between different parts of the BLR, the matter redistribution, reverberation effects, and continuum-dependent changes.

Key words. galaxies: active – galaxies: individual: Mrk 6 – galaxies: nuclei – galaxies: Seyfert

1. Introduction

The Seyfert 1.5 galaxy Markarian 6 (Mrk 6) received special attention of observers in 1971 because of strong variability of the blue hump in the broad Hβ emission line (Khachikian & Weedman 1971). Several authors in the next year (Adams 1972; Pronik & Chuvaev 1972; Ulrich 1972) revealed fast changes (over several months) in this feature. It became clear that the study of this variability needs systematic spectral observations over a long period of time. The spectral monitoring of this galaxy has been carried out at the Crimean Astrophysical Observatory with image tube spectrograph at the 2.6-m Shajn telescope from 1970–1991 by Chuvaev. From these spectra Chuvaev (1991) performed a qualitative research of the Hα and Hβ emission profiles. He marked out 5 different types of profiles that re-appeared at different times. Unfortunately he did not obtain numerical estimations from these spectra. During 1979–1982 Rosenblatt et al. (1994) also studied the spectra of Mrk 6, and the Hβ line and continuum variations. From 1992 until the present time Pronik & Sergeev have observed this galaxy with the 2.6-m Shajn telescope and with the same spectrograph used by Chuvaev, but with a CCD detector. They found (Sergeev et al. 1999) that the variations of the Hβ and Hα fluxes are delayed relative to the continuum flux variations by 18 ± 2 days and that the blue wing of the Balmer emission lines lags behind the red wing, and that some changes in the profile shape of these lines cannot be explained by the matter redistribution or reverberation effects.

Thus, there are a relatively small number of papers discussing the broad-line region (BLR) in this galaxy. We decided therefore to re-process archival image-tube spectra from 1970–1991 using new software and methods. In this paper we present results of the processing of the unique archival spectral observations of Mrk 6 from 1970–1991. Section 2 describes the observations and data reduction as well as the light curves in continuum and in the Hβ and Hα emission lines. The cross-correlation functions are discussed in Sect. 3. Relationships between different parameters of the Hβ broad profile and

Send offprint requests to: V. T. Doroshenko,
e-mail: doroshen@sai.crimea.ua

Table 1. Wavelength intervals (in observed frame) to measure fluxes.

Component	Zone, Å
F_{4825}	4802–4849
F_{5170}	5152–5196
Hβ	4850–5025
Hβ blue	4885.6–4935.1
Hβ red	4968.1–5017.6
[OIII] λ 5007	5075–5148
F_{6335}	6313–6355
F_{7030}	6985–7069
F[SII] blue	6809–6820
F[SII] red	6881–6897
Hα + [NII]	6525–6816
[SII]	6820–6878

continuum fluxes, decomposition of the broad Hβ line into two variable components, as well as the time evolution of the Hβ shape are given in Sect. 4. The results of this research are summarized in Sect. 5.

2. Observations, data processing, and light curves

Our study is based on the spectra obtained by Chuvaev with image-tube spectrograph at the 2.6-m Shajn telescope of the Crimean Astrophysical Observatory. The spectra were registered two separate spectral regions near the Hα and Hβ emission lines. The dispersion of spectrograms was about 100 Å mm^{-1}. The entrance slit width was 2–3$''$. Argon-neon lamp was used to calibrate spectra over the wavelengths. As the image tube frame covered only about 1200 Å, the spectra in these two regions have no overlapping sections and we have processed them separately. The narrow lines were taken as a calibrator of fluxes. We accepted $F([\mathrm{OIII}]\lambda\,5007) = 6.9 \times 10^{-13}$ ergs cm^{-2} s^{-1} in the Hβ region and $F([\mathrm{SII}]\ \lambda\lambda\ 6717,\ 6732) = 1.6 \times 10^{-13}$ ergs cm^{-2} s^{-1} in the Hα region (Sergeev et al. 1999). We analyzed 363 spectra for 181 dates in the Hβ region and 194 spectra for 179 dates in the Hα region. A mean spectrum of Mrk 6 combined from quasi-simultaneous observations in the Hα and Hβ spectral regions is shown in Fig. 1.

We have measured the Hα and Hβ line fluxes by direct integration over the wavelength interval above the continuum which was defined as a straight line interpolated between selected wavelength zones. The rms (root mean square) spectrum was used to look for the variable parts of emission lines as well as for selection of continuum windows and integration zones. Adopted windows are given in Table 1 and shown in Fig. 1. The integration zone for the Hβ blue wing corresponds to the radial velocity range from −4000 to −1000 km s^{-1} while the Hβ red wing was integrated from +1000 to +4000 km s^{-1}. The continuum flux was measured as the average flux within a given continuum window. The continuum light curves were computed in the two continuum window at $\lambda\lambda$ 5151–5195 Å (designated as F_{5170}) and $\lambda\lambda$ 6985–7069 Å (designated as F_{7030}).

Mean uncertainties in our measurements of fluxes are 13 and 18% for the F_{5170} and F_{7030} continua, 9 and 10% for the

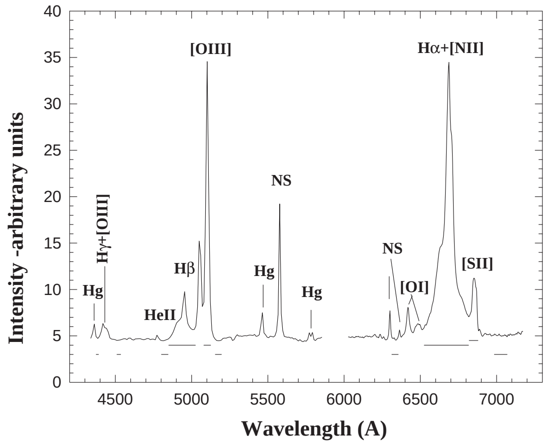

Fig. 1. Mean Mrk 6 spectrum obtained by selecting quasi-simultaneous pairs of spectra from the Hβ and Hα spectral regions. Wavelength intervals to fit the continuum and to measure the line fluxes are shown. Hg lines in the mean spectrum of Mrk 6 are light pollution due to fluorescent lamps at a distance of 200–300 m to the North of the telescope.

Table 2. Hβ region fluxes.

Julian Date −2 440 000	F^{a}_{5170}	Hβ^{b}	Hβ blue^{b}	Hβ red^{b}
892.4453	4.101	378.3	109.0	109.2
895.5508	6.269	409.8	132.0	72.72
924.5352	4.143	246.6	74.89	51.00
1039.3125	3.978	228.1	63.03	52.15
1274.5352	4.670	280.7	99.53	51.55
...	...	...	...	...
8007.2891	5.664	373.6	132.2	70.99
8540.4805	4.147	356.3	113.4	80.41

[a] Continuum flux in units 10^{-15} ergs cm^{-2} s^{-1} Å^{-1}.
[b] Emission line fluxes in units 10^{-15} ergs cm^{-2} s^{-1}.

total fluxes of the Hβ and Hα + [NII] lines, and 13 and 18% for the blue and red wings of the Hβ, respectively. The light curves of continua and emission lines are shown in Fig. 2 and given in Table 2[1]. Here we give only several rows from this table. Hereafter, we will only discuss our results in the Hβ region spectra. The ratio of the rms fluctuation to the mean flux in emission line and adjacent continuum, corrected for the effect of measurement errors is 28% and 23%, respectively in the Hβ region and 17%, 18% in the Hα region. During 1970–1991 the amplitude of flux changes in the hydrogen lines and adjacent continuum (maximum-to-minimum ratio) was about of four times. We have also calculated the light curves for the radial velocity range from −4000 to −1000 km s^{-1} in the blue wing and from +1000 to +4000 km s^{-1} in the red wing of the Hβ. The central narrow part of the Hβ emission line was excluded.

[1] Because of size, this table is only available in electronic form at `http://www.edpsciences.org`

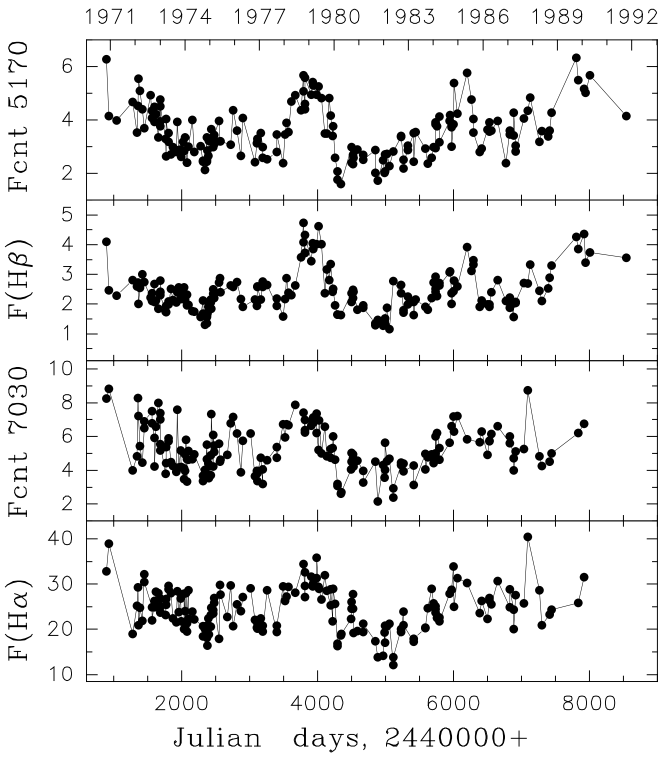

Fig. 2. Light curves for the Hβ and Hα in units 10^{-13} ergs cm^{-2} s^{-1} and for continuum at λ5170 Å and λ7030 Å in units 10^{-15} ergs cm^{-2} s^{-1} Å^{-1}.

3. Cross-correlation analysis

The cross-correlation analysis was carried out for the Hβ emission line and the continuum at 5170 Å. The cross-correlation function (CCF) was computed using the interpolation cross-correlation function (Gaskell & Sparke 1986). We computed both the lag related to the CCF peak (τ_{pk}) and to the CCF centroid (τ_{cn}), which was obtained for the correlation coefficient $r > 0.8r_{max}$. The uncertainties in the lag were found via a model-independent Monte-Carlo simulation including randomization of both the fluxes and data sampling (FR/RSS method, Peterson et al. 1998). The τ_{pk} and τ_{cn} distributions (CCPDs) were obtained from 1000 independent realizations of CCF. The uncertainties computed directly from the CCPDs were referred to the 68% confidence level that corresponds to $\pm 1\sigma$ for a normal distribution. The CCFs for the total Hβ flux and Hβ wings are shown in Fig. 3. We found the τ_{pk} to be 13^{+15}_{-20} and τ_{cn} to be 14^{+25}_{-21}. Both values are consistent with those obtained by Sergeev et al. (1999): $\tau_{pk} = 18 \pm 2$ days. Unfortunately, the quoted uncertainties are very large. In particular, we can say nothing about BLR kinematics in Mrk 6 from our blue and red wing CCFs.

4. Structure and evolution of the Hβ profile

4.1. Variability patterns of the Hβ broad line profile

An earlier study by Chuvaev (1991) that was based on the same spectral material revealed strong changes in the Hβ emission-line profile. Sometimes, the Hβ had broad wings as in Sy 1 type

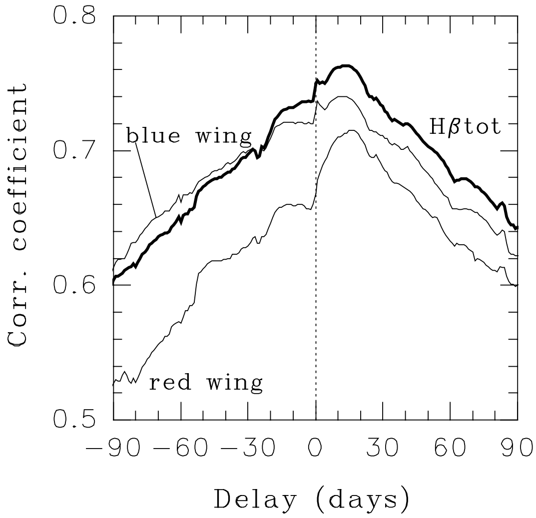

Fig. 3. Cross-correlation functions between Hβ and continuum at λ5170 Å (thick line) and between the Hβ wings and continuum (thin lines).

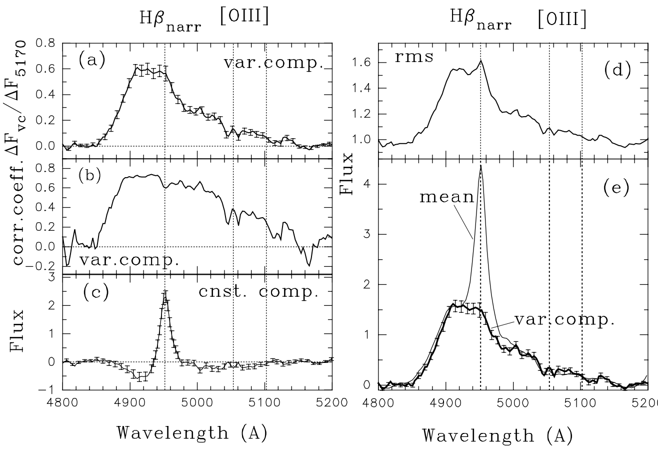

Fig. 4. Decomposition of the Hβ profile into variable (panel **a)**) and constant component (panel **c)**). The mean and rms spectra are shown in panels **e)** and **d)**, respectively. The coefficient of correlation at different wavelengths of the line profile between the line and continuum at λ 5170 Å is shown in panel **b)**. Flux is given in units 10^{-15}ergs cm^{-2} s^{-1} Å^{-1}.

galaxies, and, sometimes, the wings were relatively weak, similar to those in Sy 2 galaxies. The changes were detected not only in the Hβ fluxes but also in the Hβ profile.

In the simplest case we can consider the situation in which there are two components in the line profile: the first component is a constant in flux and shape and the second is a single variable component, the flux of which linearly depends on the observed continuum flux, but it is constant in shape. In such a case we can obtain a single solution for the profile shape of these components (Sergeev et al. 1994). We have calculated the profiles of both components for our data set. The results are shown in Fig. 4.

Figure 4a illustrates the increment of the variable component when the change in the continuum flux at F_{5170} equals unity. The constant component of the Hβ emission-line profile is shown Fig. 4c. The profile of the variable component is very

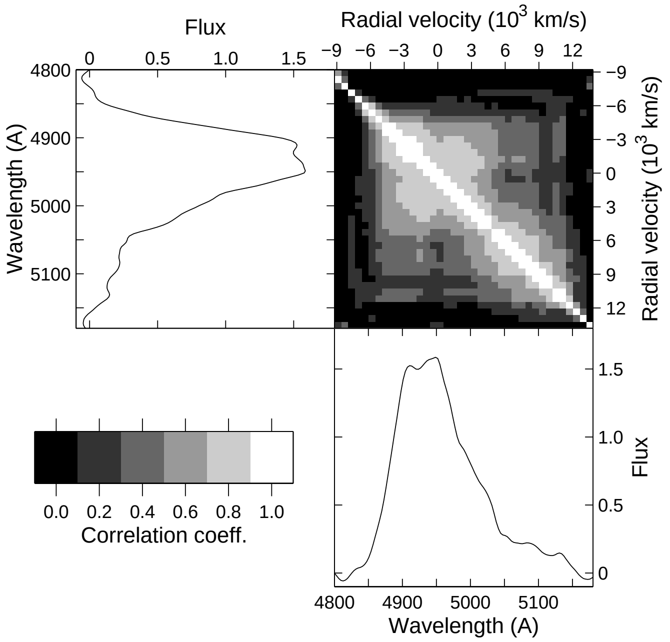

Fig. 5. Correlation matrix for the Hβ line profile. This matrix contains the correlation coefficients between pairs of the light curves for all profile bins. By definition, a correlation coefficient is equal to unity for its main diagonal.

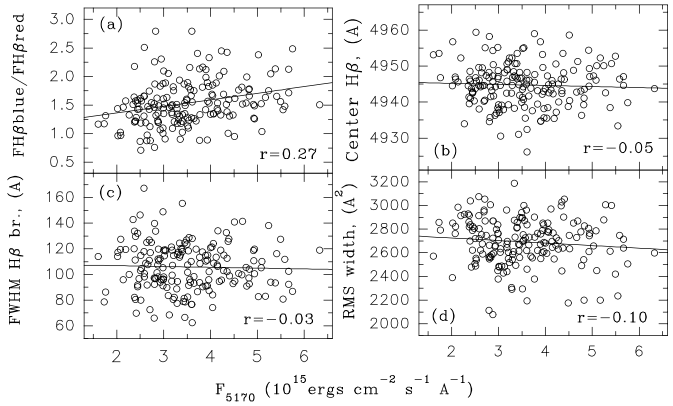

Fig. 6. Relationship between the continuum flux F_{5170} and **a)** the broad component ratio of fluxes in the Hβ blue window (−3000, −1000 km s^{-1}) to the Hβ red window (+1000, +3000 km s^{-1}); **b)** the centroid of the broad Hβ emission line profile; **c)** FWHM of the broad Hβ emission line profile; and **d)** rms width.

similar to the rms profile given in panel d. The correlation coefficient computed for a set of the profile segments shows that the blue part of the broad component correlates better with the optical continuum than the red part (Fig. 4b). The variable broad line component seems to be very asymmetric: it has a strong and sharp blue bump and less intensive but more extended red wing. The profile centroid is shifted to the blue side. A bump in the red wing of the Hβ sometimes appeared. For example, it is seen in spectra at JD 2 443 500–3700 in Fig. 11.

The narrow emission line component of Hβ was subtracted from the total Hβ line profile. The narrow lines of the spectra were optimally aligned in wavelength and spectral resolution before. The mean Hβ broad emission line profile is shown in Fig. 5. The correlation matrix is shown in this figure. It contains the correlation coefficients between pairs of the light curves for all profile bins. The profile segments with poor correlation have a dark color. The main diagonal, where the correlation coefficient $r = 1$, by definition, is white. We can see that the central part of the profile correlates poorly with other profile segments, especially with the segments at the radial velocities more than 4000 km s^{-1}, while the profile segment with the radial velocity near −3000 km s^{-1} has a good correlation with profile segments from +1000 to +3000 km s^{-1}.

Further, we looked for how the other parameters of the broad Hβ emission line are dependent on the continuum flux. We considered the profile centroid of the broad Hβ line, the full width at half intensity – FWHM, the root mean square width (also referred to as profile dispersion or rms width), and the ratio of the blue wing flux (−3000, −1000 km s^{-1}) to the red wing flux (+1000, +3000 km s^{-1}). All these parameters were computed for the broad Hβ profile from which the narrow component has been subtracted. We show these relations in Fig. 6.

From Fig. 6 we can see that the centroid and FWHM do not depend on the continuum flux, while the ratio of the blue wing flux to the red wing flux has a weak tendency to increase with the increasing continuum flux ($r = 0.27$). The rms width also shows a very weak tendency to decrease with an increase in the continuum flux ($r = 0.10$).

4.2. Emission-line shape

The broad emission line profile in Mrk 6 shows changes not only in flux, but also in shape. We can demonstrate changes in shape in different ways. At first, to clarify interrelation between profile shape and continuum flux we distributed all spectra into three groups: a high state continuum flux (4.53–6.33, 28 spectra), an intermediate state (3.16–4.53, 84 spectra), and a low state (1.61–3.16, 69 spectra), where units are 10^{-15} ergs cm^{-2} s^{-1} Å^{-1}. The mean profile of the Hβ broad component in each of these states is shown in Fig. 7a. In the bottom panel of Fig. 7 we show the same profiles normalized in such a way that the total flux is equal to unity for each profile. While the entire Hβ broad line profile increases with the continuum brightening (Fig. 7a), the patterns of the normalized profiles show little, if any, dependence on the continuum flux. In general, the normalized profiles seem to be remarkably similar each to other, although as the continuum flux brightened, the blue wing of the Hβ line (radial velocities from −3000 km s^{-1} to 0 km s^{-1}) increases a little with respect to other profile segments, while the red wing (radial velocities from +1000 km s^{-1} to +3000 km s^{-1}) decreases. In order to obtain a quantitative estimation of the profile evolution and its dependence on the continuum flux we considered, hereafter, the two profile segments at ±(1000–3000) km s^{-1}. These two segments are shown by dotted lines in Fig. 7.

A more detailed consideration of the changes in the Hβ broad line profile was done following Wanders & Peterson (1996). The word "shape" was used by them when they take

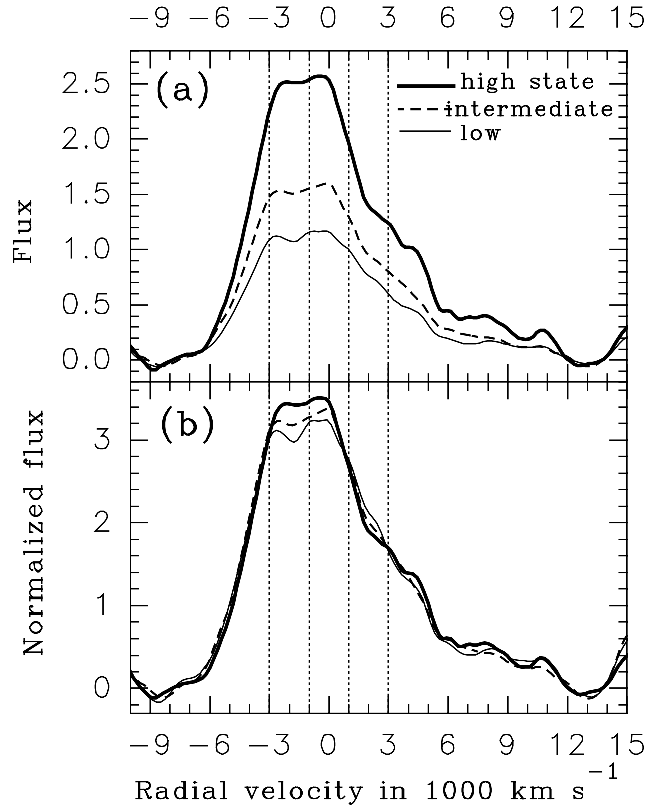

Fig. 7. a) Averaged profile of the Hβ emission line in high, intermediate, and low states of activity in units 10^{-15} ergs cm^{-2} s^{-1}, and **b)** the same profiles normalized so that its integrated flux equals to unity.

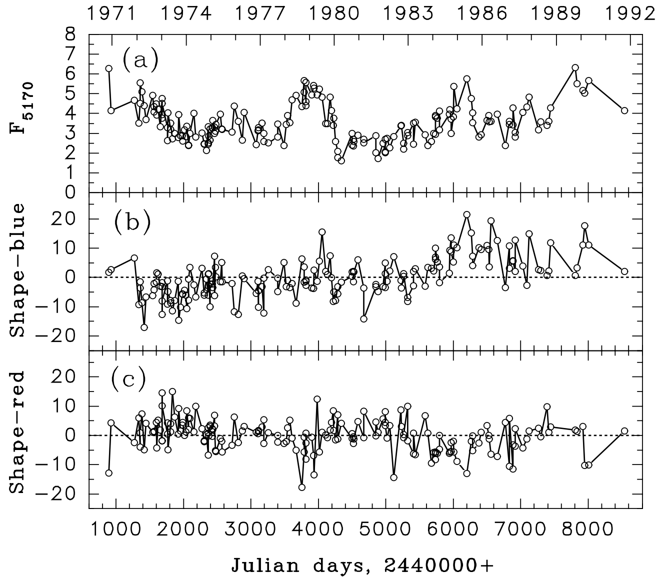

Fig. 8. a) Light curve for the continuum flux F_{5170} and curves for **b)** the blue $(-3000, -1000$ km s$^{-1})$ and **c)** the red $(+1000, +3000$ km s$^{-1})$ shapes. Fluxes are given in units 10^{-15} ergs cm^{-2} s^{-1}.

into consideration a relative prominence of a given profile segment. The "shape" is computed as follows:

$$Fq(v,t) = F(v,t) - \frac{\langle F(v) \rangle}{\langle F(t) \rangle} \cdot F(t),$$

where $F(v,t)$ is the flux of emission line at the velocity v and time t, $F(t)$ is the total flux over the entire emission line for time t, and angled brackets denote time average. It follows from the equation that $Fq(v,t)$ will be close to zero when a given profile segment $F(v,t)$ changes proportionally to the total flux $F(t)$. If the proportionality will be disturbed due to delay effects or other reasons, the $Fq(v,t)$ will be positive or negative. So, the $Fq(v,t)$ is sensitive to the relative prominence of certain parts of the emission line.

We considered two shape time series corresponding to the blue (from −3000 to −1000 km s^{-1}) and red (from +1000 to +3000 km s^{-1}) segments of the Hβ emission line. In these segments, profile shapes vary more appreciably. The time series are presented in Fig. 8. It is clearly seen that the behaviour of the blue and red shapes is different.

The relations between fluxes and shapes of the Hβ blue and red parts are shown in Fig. 9. There is high correlation between the fluxes of the blue and red parts of the broad Hβ emission line ($r = 0.81$, Fig. 9a). At the same time, there is an anti-correlation ($r = -0.47$) between shape of the Hβ blue and red segments (Fig. 9b).

The shape of the Hβ blue segment is weakly correlated with Hβ total flux ($r = 0.20$, Fig. 9c), and continuum flux F_{5170} ($r = 0.24$, Fig. 9e), while the shape of the Hβ red segment shows anti-correlation with the Hβ total flux ($r = -0.28$, Fig. 9d) and continuum flux ($r = -0.28$, Fig. 9f).

So, we can conclude that the shape variations do not follow the flux variations and they are not induced by the continuum variations. Such behaviour can take place when the different parts of a profile have a different delay, or when profile variations are not connected with the reverberation effect, but the line emission is redistributed in physical and velocity space. Possibly, the BLR consists of several components that manifested themselves at different times for some reason.

4.3. Decomposition of the Hβ broad emission line into two variable components

The complicated behaviour of the profile shape of the Hβ broad component described above allowed us to assume that the observed broad profile consists of at least two components with a fixed profile but with variable relative strength. In such a case the observed line profile $F_{\lambda,t}$ can be written as

$$F_{\lambda,t} = S1_{\lambda} F1_t + S2_{\lambda} F2_t$$

where $S1_{\lambda}$ and $S2_{\lambda}$ are the profile shapes of the first and second component, and $F1_t$ and $F2_t$ are their light curves. Each profile shape is normalized such a way that its integrated flux is equal to unity. These equations can be solved using the least squares method. The solutions with negative values for S_{λ} and F_t are excluded. We have subtracted the narrow component from the Hβ emission line profile and solved the equation assuming that there are only two variable components in the broad line. We have found that the approximation accuracy (rms) for this model is better by 15% than that for the model considered in Sect. 4.1. In Fig. 10 a continuous set of possible solutions is shown discretely. Possible solutions for one component are shown by the dashed line, while possible

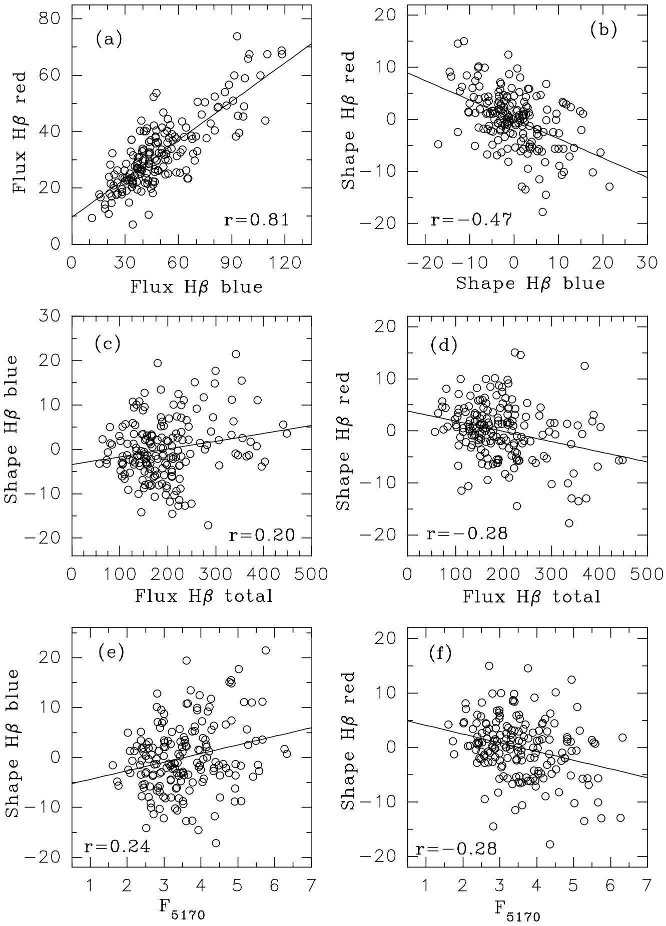

Fig. 9. Flux-flux, flux-shape and shape-shape diagrams for the blue and red segments of the broad Hβ emission line. Fluxes are given in units 10^{-15} ergs cm^{-2} s^{-1}.

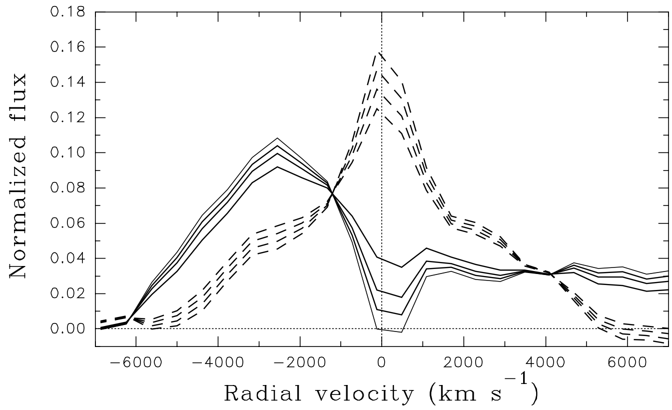

Fig. 10. Possible solutions for the profiles of the first and second components are shown by dashed and solid lines, respectively. A continuous set of solutions is shown discretely, including upper and lower bound solutions for each component.

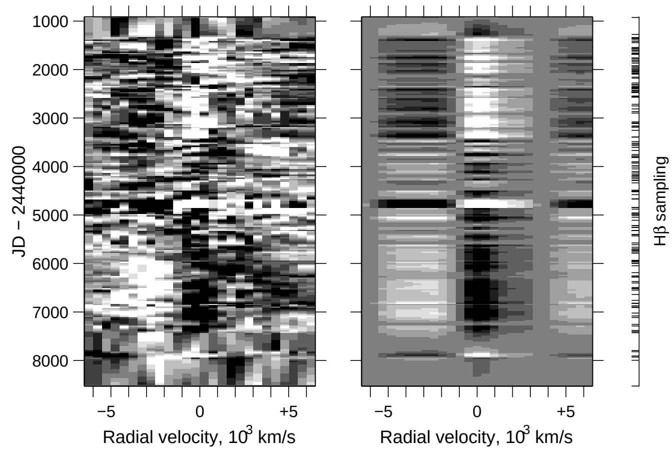

Fig. 11. Evolution of residuals between normalized profiles and mean normalized profile is shown as a two-dimensional image for the Hβ emission line. Bright regions indicate that the normalized profile for this time and wavelength is higher than the mean normalized profile, while dark regions demonstrate where and when it is lower. The right panel presents the same image reproduced by fitting the observed Hβ profile in terms of a model with two variable broad components. The times of actual observations are indicated on the right.

solutions for another component are shown by the solid line. The component shown by the dashed line is almost symmetric and has a central peak, while the other component has a blue peak and extended red tail. The described decomposition of the Hβ broad line into two components was done for each observational date and evolution of this fitting is shown in Fig. 11 – right panel.

4.4. Evolution of the Hβ profile

The changes in the line profile can also be illustrated using a two-dimensional image. In order to construct this image we have normalized all profiles to a constant arbitrary flux after subtraction of the narrow emission component of Hβ. Next we have subtracted a mean normalized profile from each individual normalized profile. The residuals were rebinned over time and over wavelength, and these residuals are shown in Fig. 11.

Bright regions of this image indicate that the normalized profile for this time and wavelength is higher than the mean normalized profile, while dark regions mark lower intensity than the mean profile. The normalized profile of the Hβ shows complicated behaviour over time and wavelength that cannot be attributed to noise because it occurred over time and wavelength intervals which are much larger than our time and wavelength resolutions. There are regions with strong red wings, but with a weak blue part of the profile. There is a time period when the central part is bright while both wings are weak, and there is a state when the blue wing increased, whereas both the central part and red wing weakened. In many cases, the red part of the profile is weak when the blue wing is bright and vice versa. The anti-correlation between shapes in the blue and red parts of the profiles is also very well seen in Fig. 9b or in Fig. 8 during the time interval JD 2 444 700–2 446 200 when the blue wing shape increases monotonically (and total flux is also increasing), whereas the red wing shape is not.

On the right panel of Fig. 11 the same image is shown reproduced by fitting the observed Hβ profile in terms of a model with two variable components (see also Fig. 10). In general, this model reproduces the principal details in the observed picture on the left panel, e.g. such as dominating the central part of the profile for JD 2 441 200–2 443 200, JD 2 444 800–2 444 900 and JD 2 446 300–2 447 200 days, and a strong blue part of the profile during JD 2 445 900–2 447 100 days. But, in general, the observed evolution of the Hβ profile is much more complicated than the fitting model.

5. Summary

More then twenty years of optical spectral monitoring of the nucleus of Mrk 6 revealed that:

- The light curves in the Hβ and Hα lines and also in the adjacent continuum show appreciable variability. The ratio of the rms fluctuation to the mean flux in emission lines and in the adjacent continuum, corrected for the effect of measurement errors, is 28% and 23%, respectively, in the Hβ region, and 17% and 18% in the Hα region.
- We studied the relationship between broad-line profile parameters (such as centroid, width, and blue-to-red ratio of fluxes) and continuum flux. We found that the centroid and FWHM do not depend on the continuum flux, while the ratio of the blue wing flux to the red wing flux has a weak tendency to increase with an increase in the continuum flux ($r = 0.27$). The rms width also shows very weak tendency to decrease with an increase in the continuum flux ($r = 0.10$).
- We studied correlations between fluxes and shapes of the blue (-3000 to $-1000\,\mathrm{km\,s^{-1}}$) and red ($+1000$ to $+3000\,\mathrm{km\,s^{-1}}$) wings of the H$\beta$, as well as correlations between shapes in wings, on the one hand, and Hβ total and continuum fluxes, on the other hand (Fig. 9). The red and blue fluxes show a high degree of correlation. Anti-correlation between blue and red shapes of the Hβ, positive correlation between the blue shape and line/continuum flux, and anti-correlation between the red shape and line/continuum flux shows that the blue segments respond slightly better to the continuum changes than the red segment and total Hβ line. In terms of a power dependence between line and continuum fluxes, it may indicate larger power index for the blue segment of the Hβ line.
- In terms of the two-broad-component profile model, a set of the observed Hβ profiles can be reproduced, although not so well defined, by changes in the relative strength of the two variable components with fixed profiles (Figs. 10 and 11). We found that one of the broad components is single-peaked and almost symmetric, while the other component has a blue bump and extended red wing.
- The evolution of the broad Hβ profile in Mrk 6 (as well as in many other AGNs) is complicated and not clear at all. The evolution is driven, most likely, by a set of various factors, including a multi-component BLR model in which different parts of the BLR manifested themselves at different times (e.g., due to redistribution of ionizing radiation between different parts of the BLR), matter redistribution, reverberation effects, and continuum-dependent changes.

Acknowledgements. This research was supported by RBRF (Russian Foundation for Basic Research) No. 00-02-16272 and CRDF (US Civilian Research & Development Foundation) award No. UP1-2116.

References

Adams, T. F. 1972, ApJ, 172, L101
Chuvaev, K. K. 1991, Izvestia Krymskoy Astrofizicheskoy Observatorii, 83, 194
Gaskell, C. M., & Sparke, L. S. 1986, ApJ, 305, 175
Khachikian, E. Y., & Weedman, D. W. 1971, ApJ, 164, L109
Peterson, B. M. Wanders, I., Horne, K., et al. 1998, PASP, 110, 660
Pronik, V. I., & Chuvaev, K. K. 1972, Astofizika, 8, 187
Rosenblatt, E. I., Malkan, M. A., Sargent, W. L. W., et al. 1994, ApJS, 93, 73
Sergeev, S. G., Malkov, Yu. F., Chuvaev, K. K., et al. 1994, in Reverberation mapping of the broad-line region in active galactic nuclei, ed. P. M. Gondhalekar, K. Horne, & B. M. Peterson (San Francisco: ASP), ASP Conf. Ser., 69, 199
Sergeev, S. G., Pronik, V. I., & Sergeeva, E. A. 1999, ApJS, 121, 159
Wanders, I., & Peterson, B. M. 1996, ApJ, 466, 174
Ulrich, M. H. 1972, ApJ, 171, L35